Available online at www.sciencedirect.com

Chemical Engineering Research and Design

journal homepage: www.elsevier.com/locate/cherd

Two-phase stratified flow in horizontal pipes: A CFD study to improve prediction of pressure gradient and void fraction

*Stefano Passoni**, *Igor Matteo Carraretto*, *Riccardo Mereu*, *Luigi Pietro Maria Colombo*

Department of Energy, Politecnico di Milano, via Lambruschini 4a, 20156 Milan, Italy

ARTICLE INFO

Article history:
Received 22 October 2022
Received in revised form 9 January 2023
Accepted 9 January 2023
Available online 13 January 2023

Keywords:
CFD
VOF
Interface Tracking
Two-phase
Stratified flow
Pressure drop

ABSTRACT

Improved understanding of flow regime effects on design-influencing engineering quantities is of primary importance. This work is focused on the numerical prediction of pressure gradient and void fraction in a horizontal pipe where gas-liquid stratified flow is present in different operating conditions. The problem was modeled with unsteady, multiphase CFD (computational fluid dynamics) simulations. Volume Of Fluid (VOF) method was used as multiphase model. To define the numerical methodology, this study provides details on the influence of discretization grid and turbulence model on the simulation accuracy. It shows that mesh density on pipe cross-section is the most important grid parameter to focus on. Different turbulence models are required depending on the gas velocity and on its turbulence flow regime. Transition SST is able to model all the operating conditions but Realizable k-ε is adopted to further increase the accuracy of the results. A general underestimation of the pressure gradient is reported with an average error of – 6.43 % and – 16.21 % for a liquid superficial velocity of 0.04 m/s and 0.06 m/s respectively. Comparison with two-fluid 1D models shows that CFD simulations are the most accurate tools for predicting the pressure gradient at gas superficial velocities lower than 1.3 m/s. The implementation of a drift flux model shows a good agreement between experimental results and CFD simulations concerning void fraction estimation. CFD results are also used to underline the physical phenomena limiting the performance of 1D models.

1. Introduction

In the last decades, the industrial relevance of multiphase flows has grown significantly (Brennen, 2005). Among all the possible flow regimes, stratified two-phase flow in horizontal pipelines is relevant in oil and gas transportation pipelines, for example, where the accurate prediction of pressure drop is essential for the pipeline design itself (Mokhatab and Poe, 2012). Improved understanding of the effects flow regime has on quantities like flow rate and pressure is therefore of primary engineering importance. The conditions of existence of stratified flow have been widely investigated both experimentally – leading to flow pattern maps – and theoretically – in terms of transition criteria. For the purposes of this work, it is worth mentioning the flow pattern map proposed by Mandhane et al. (1974) based on data for horizontal gas-liquid flows, which adopts the superficial velocities of the phases with simple parameters to account for fluid property variations. Their correlation was derived from nearly 6000 flow pattern observations available in the UC Multiphase Pipe Flow Data Bank. From the theoretical point of view, a

* Corresponding author.
E-mail addresses: stefano.passoni@polimi.it (S. Passoni), igormatteo.carraretto@polimi.it (I.M. Carraretto), riccardo.mereu@polimi.it (R. Mereu), luigi.colombo@polimi.it (L.P.M. Colombo).

https://doi.org/10.1016/j.cherd.2023.01.016

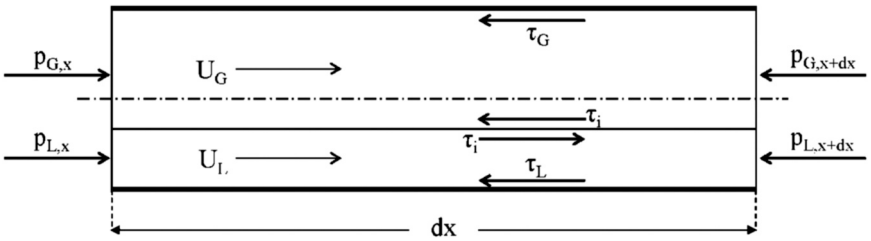

Fig. 1 – Two-fluid force balance on pipe section of length *dx* (Carraretto et al., 2020).

detailed characterization of stratified/nonstratified transitional boundaries based on stability analyses has been provided by Brauner (1991).

On the other hand, focusing on modeling, the simplest approach is based on one-dimensional, steady-state two-fluid models for which the momentum balance can be solved to derive both the frictional pressure gradient and the phases volume fraction. The mathematical formulation for each phase is reported in equation (1) referring to the force balance illustrated in Fig. 1.

$$\left[p_x - \left(p_x + \frac{dp}{dx}dx\right)\right]\Omega_{g/L} - \tau_{g/L}S_{g/L}dx \mp \tau_i S_i dx = 0 \tag{1}$$

With some algebraic steps, the expressions of pressure gradient are obtained:

$$-\frac{dp}{dx} = \tau_g\frac{S_g}{\Omega_g} + \tau_i\frac{S_i}{\Omega_g} \tag{2}$$

$$-\frac{dp}{dx} = \tau_L\frac{S_L}{\Omega_L} - \tau_i\frac{S_i}{\Omega_L} \tag{3}$$

Where S is the wetted perimeter, Ω is the cross section and τ is the phase wall shear stress, each of these three quantities is referred to the two phases.

It is seen that the two momentum balances are linked by the interfacial shear stress, τ_i, usually computed from the interfacial friction factor, which in most cases is correlated to the gas Reynolds number. This is a crucial quantity as it describes the interaction between the phases at the interface. As a consequence, various models have been proposed in the literature, mostly differing in the expression of the interfacial shear.

Specifically, regarding stratified gas-liquid flows in horizontal pipes, several authors during the years worked on different 1D models. Cohen and Hanratty (1968) studied experimentally the properties of the interfacial waves in a flat channel (12" wide and 1" high) with fully developed flows of air and water or air and glycerine in water solutions. The liquid flow was always laminar, with a Reynolds number (based on the bulk velocity and the height of the liquid film) ranging between 190 and 620. Instead, the air stream was always turbulent, with bulk velocities in the range 5–30 ft/s (about 1.5–9 m/s). The effective shear stress at the interface was calculated from the pressure drop and the distance of the maximum in the gas velocity profile from the interface by using a force balance. Two types of wave structures are observed: two-dimensional and three-dimensional waves. Waves heights were measured optically and the amplitude distribution function turned out to be quite accurately approximated by a Gaussian distribution. The interfacial friction factor was then evaluated and an equivalent sand roughness for the liquid-air interface was calculated by comparison with the Nikuradse's equation for the completely rough regime. Three-dimensional waves were found to behave similarly to fully rough solid surfaces with a marked dependence of the interfacial friction factor on the root-mean-square wave height.

Govier et al. (1973) provided a standard formulation of the two-fluid model, suggesting that the wall shear stress of each phase be calculated from single-phase correlations, whereas the correlation by Ellis and Gay (1959) was adopted for the interfacial shear stress in two forms: one for smooth and one for wavy interface, respectively.

Agrawal et al. (1973) refined the two-fluid model reported by Govier and Aziz (1972) with two major modifications. First, they removed the assumption that the interface behaves as a stationary surface relative to the liquid phase by deleting the interface perimeter from the definition of the hydraulic diameter for the liquid phase. Second, the friction factor of the liquid phase was (arbitrarily) evaluated by assuming a velocity profile in the liquid layer, i.e. a portion of the profile, which would exist if the pipe were filled with the liquid. This requires the numerical evaluation of an integral. Differently, single-phase flow correlations were used for the friction factor of the gas. The whole procedure is iterative and starts with assuming the liquid holdup. Considering the interface hydrodynamically smooth, the empirical correlation of Ellis and Gay (1959) was adopted for the interfacial shear stress. The model predictions were validated against an experimental database of air-(light) oil flows in a 1" (2.54 mm) i.d. acrylic pipe, showing satisfactory performance.

Taitel and Dukler (1976) formulated the two-fluid model according to Govier et al. (1973) apart from introducing the definition of the hydraulic diameter for the liquid phase proposed by Agrawal et al. (1973). Their major contribution was devoted to find the transition criteria between stratified and intermittent or annular-dispersed liquid regimes based on stability criteria for waves according to the Kelvin-Helmholtz theory. They always assume that the interfacial friction factor is practically equal to the friction factor of the gas phase, which should apply for a solid, stationary and smooth interface. They state that in spite many of the transitions take place in stratified flow with a wavy interface, this assumption leads to small errors. Their model as well as the expressions of the dimensionless liquid height as a function of the Lockhart-Martinelli parameter are reported in several handbooks as a customary approach to stratified flows.

Cheremisinoff and Davis (1979) implemented a two-fluid model for stratified turbulent-turbulent gas-liquid flow with some modifications with respect to the previous approaches. In particular, they extended the model of Russell et al. (1974) to the turbulent liquid phase by application of eddy viscosity expressions developed for single-phase flow, stating that the advantage of this type of modeling relies on the possible extension to heat transfer predictions in view of the analogy between momentum transfer and heat transfer. Single-

phase flow correlations were instead used for the friction factor of the gas. The interfacial friction factor was taken from Cohen and Hanratty (1968) to account for three-dimensional waves and from Miya et al. (1971) for roll waves. The resulting iterative procedure is similar to the one proposed by Agrawal et al. (1973). The model predictions were compared with data for air-water flow in a smooth tube of 63.5 mm i.d. (Re_g = 11000–50000, Re_L = 5000–18000) and other data from the literature. The average deviations on the pressure drop were 24.3 % and 26.4 % for small amplitude interfacial waves and roll waves, respectively. Such a performance resulted far superior to the prediction by the Lockhart-Martinelli (Lockhart, 1949) separated flow model.

Kowalski (1987) provided measurements of the interfacial shear stress in stratified gas-liquid flow in a Lexan pipe, 50.8 mm i.d. (Re_g = 24260–56870, Re_L = 17490–36560). The gas was either air or Freon-12 and the liquid was always water. The two-fluid model was used to determine the interfacial shear stress from the measurements of the wall shear stresses of the two phases and of the void fraction. Alternatively, the interfacial shear stress was extrapolated from the Reynolds shear profile at the gas-liquid interface. The two methods showed consistent results. Empirical correlations were provided for smooth and wavy stratified flow. In the former case, disagreement was found with the correlation of Ellis and Gay (1959) suggested by Agrawal et al. (1973).

Crowley et al. (1992) focused on the transition between stratified and slug flow regime in pipes developing a complete solution methodology for the one-dimensional wave approach. The analysis aimed at outdoing the empiricism inside the Taitel and Dukler (1976) model and was validated against experimental data for pipes with 0.0254–0.30 m i.d., in a broad range of superficial velocities and gas pressures from nearly atmospheric to about 30 times higher. Moreover, data for downwardly inclined pipes (– 0.057° to – 2°) were also considered. The equilibrium solution was based on the two-fluid model where the same constant value of 0.005 was taken for the friction factors of each phase and the interfacial friction factor assuming that the flow regime transition is not very sensitive to the selection of the friction factors. This enabled solving the system of the two momentum equations without iterations.

Ullmann and Brauner (2006) proposed a new, theory-based set of closure relations for the wall and interfacial shear stresses applicable to turbulent flows in the phases. This work is an extension of the method proposed by Ullmann et al. (2004) for laminar flows. The goal of the work was to overcome the limitations due to the use of single-phase-based closure relations for the two-fluid model. Accordingly, the latter were modified in order to include correction terms for the wall shear stresses, which embody the effects of variations of the effective hydraulic diameters due to the interaction between the phases. In particular, they noticed that even in the smooth stratified flow regime, where the interface is practically flat, the conventional closure relations may lead to inaccurate predictions of both the pressure drop and phase holdups. Validation was provided using four databases including mostly air-water flows in pipes with 51–18 mm i.d. and inclinations between 0° and 3° (upwards/downwards). More recently, a few papers have been published on two-phase stratified flow, where researchers have devoted their attention to either wavy flow (characterizing the wave parameters, i.e. Tzotzi et al., 2011) or transition to intermittent flow (i.e. plug/slug, i.e. Arabi et al., 2021).

To achieve a more detailed description, full 3D modeling by means of Computational Fluid Dynamics (CFD) is required. A typical approach for the simulation of two-phase stratified flows consists in using the Reynolds-averaged Navier-Stokes (RANS) equations with the Volume Of Fluid (VOF) Model for interface tracking. Banerjee and Isaac (2003) applied three different turbulence models (standard k-ε, RNG k-ε, and Reynolds Stress Model) in conjunction with VOF model. Their results showed that standard k-ε and RNG k-ε matched the experiments more accurately. Also, RNG k-ε gave the overall best results compared to the other two models. de Sampaio et al. (2008) numerically investigated two-phase stratified flow in horizontal pipe using the k-ω turbulence model. They compared the results against available experiments and 1D model by Taitel and Dukler (1976). The authors showed that k-ω model is able to model such flow regimes and highlighted the importance of the turbulence quantities' interfacial value. Dabirian et al. (2015) simulated air-water flow in horizontal pipeline and compared the results against experiments and 1D correlation described in Taitel and Dukler (1976). They adopted the Realizable k-ε and VOF models using a commercial solver. Given the small discrepancy with experimental data, their validation concluded that CFD simulations have the potential to be considered a valuable design tool in petroleum industry. Chinello et al. (2018) compared the use of SST k-ω turbulence model with and without damping of the turbulence at the interface by benchmarking the results against experimental pressure drop and liquid hold-up. They concluded that although applying damping influences the agreement with experiments, RANS with SST k-ω has shown some limitations on accurately predict the presence of waves at the interface.

In this paper, unsteady RANS-based CFD simulations with VOF multiphase model are used to model gas-liquid stratified flow in horizontal pipes. For validation purposes, simulation results are compared to an experimental study done at Multiphase Thermo-Fluid Dynamics Laboratory at Politecnico di Milano by Carraretto et al. (2020) and to several 1D models (Cohen and Hanratty, 1968; Agrawal et al., 1973; Taitel and Dukler, 1976; Cheremisinoff and Davis, 1979; Kowalski, 1987; Crowley et al., 1992; Ullmann and Brauner, 2006). The main purpose of this paper is to present a numerical methodology to accurately predict the pressure gradient and the void fraction by means of fluid dynamic simulations. Moreover, the numerical results are post-processed to emphasize the physical phenomena limiting the prediction capability of 1D two-fluid homogeneous models. The plan of the paper is as follows: in Section 2 the governing equations of an unsteady multiphase problem, a description of the domain and discretization grid considered for the numerical analysis, the solver setup and validation procedure are reported. In Section 3 the sensitivity analyses needed to define the simulation methodology and the validation of the numerical results are presented. In Section 4 the CFD results are further commented, elaborated and compared to 1D homogeneous models. Lastly, in Section 5 the conclusions of the present work are drawn.

2. Numerical model

2.1. Governing equations

In this paper the Volume Of Fluid (VOF) model is employed to model two immiscible phases, air and water. When employing this model, a single set of momentum conservation

equations and one continuity equation are shared by the fluids and each volume fraction is tracked throughout the domain with a continuity equation. Defining the volume fraction of phase n as

$$\alpha_n = \frac{V_n}{V} \tag{4}$$

where V_n is the volume of phase n in a cell of volume V, its transport equation assuming constant fluid density and no mass transfer between phases is given by

$$\frac{\partial \alpha_n}{\partial t} + \nabla\cdot(\alpha_n \vec{v}) = 0 \tag{5}$$

In a two-phase system, this equation is solved only for the second phase while the volume fraction of the first one is computed given the constraint of $\alpha_1 + \alpha_2 = 1$. The mixture density and viscosity are given by $\rho = \alpha_2\rho_2 + (1-\alpha_2)\rho_1$ and $\mu = \alpha_2\mu_2 + (1-\alpha_2)\mu_1$, respectively. Specific algorithms for interpolation near interface are also used within multiphase models to provide good accuracy for interface shape.

The equations for mass and momentum conservation can be written as:

$$\frac{\partial \rho}{\partial t} + \nabla\cdot(\rho\vec{v}) = 0 \tag{6}$$

$$\frac{\partial}{\partial t}(\rho\vec{v}) + \nabla.\,(\rho\vec{v}\,\vec{v}) = -\nabla p + \nabla.\,(\bar{\tau} + \bar{\tau}_t) + \rho\vec{g} + \vec{F} \tag{7}$$

where F is a force term that can be used to model the influence of surface tension, $\bar{\tau}$ is the molecular stress tensor, and $\bar{\tau}_t$ is the turbulent stress tensor (Reynolds Stress).

Regarding turbulence models, the Transition SST, SST k-ω and Realizable k-ε models are used to model turbulence in this study. The first is used for low gas superficial velocities while the second is employed for the highest ones, when a fully turbulent flow regime is clearly present. The Transition SST model (also known as γ-Re_θ model) is a modification of the SST k-ω model by Menter (1994) which is coupled with two more transport equations: one for the *intermittency* (γ) and one for the *Transition Momentum Thickness Reynolds number* ($Re_{\theta t}$). According to ANSYS (2019), the equation solved when adopting this model are:

$$\frac{\partial}{\partial t}(\rho k) + \frac{\partial}{\partial x_i}(\rho k U_i) = \frac{\partial}{\partial x_j}\left(\Gamma_k \frac{\partial k}{\partial x_j}\right) + G_k^\star - Y_k^\star \tag{8}$$

$$\frac{\partial}{\partial t}(\rho\omega) + \frac{\partial}{\partial x_i}(\rho\omega U_i) = \frac{\partial}{\partial x_j}\left(\Gamma_\omega \frac{\partial k}{\partial x_j}\right) + G_\omega - Y_\omega \tag{9}$$

$$\frac{\partial}{\partial t}(\rho\gamma) + \frac{\partial}{\partial x_i}(\rho\gamma U_i) = P_{\gamma 1} - E_{\gamma 1} + P_{\gamma 2} - E_{\gamma 2} + \frac{\partial}{\partial x_j}\left[\left(\mu + \frac{\mu_t}{\sigma_\gamma}\right)\frac{\partial \gamma}{\partial x_j}\right] \tag{10}$$

$$\frac{\partial}{\partial t}(\rho Re_{\theta t}) + \frac{\partial}{\partial x_i}(\rho Re_{\theta t} U_i) = P_{\theta t} + \frac{\partial}{\partial x_j}\left[\sigma_{\theta t}(\mu + \mu_t)\frac{\partial Re_{\theta t}}{\partial x_j}\right] \tag{11}$$

Eqs. (8) and (9) are the same of the SST k-ω model. In these equations, the terms with G and Y represent respectively the production or the dissipation of turbulent kinetic energy (k) and specific rate of turbulence dissipation (ω). Equations (10) and (11) are instead the ones that give the model the ability of predicting the laminar-turbulent transition. In these equations, the terms $P_{\gamma 1} - E_{\gamma 1}$ and $P_{\gamma 2} - E_{\gamma 2}$ represent, in order, the transition and the relaminarization sources. The transition model interacts with the SST turbulence model through a modification of the k-equation production and dissipation sources ($G_k^\star - Y_k^\star$).

The Realizable k-ε model (Shih et al., 1995) is, instead, a fully turbulent model characterized by the following transport equations for the turbulent kinetic energy and turbulence dissipation (ε)

$$\frac{\partial}{\partial t}(\rho k) + \frac{\partial}{\partial x_i}(\rho k U_i) = \frac{\partial}{\partial x_j}\left[\left(\mu + \frac{\mu_t}{\sigma_k}\right)\frac{\partial k}{\partial x_j}\right] + G_k - \rho\varepsilon \tag{12}$$

$$\frac{\partial}{\partial t}(\rho\varepsilon) + \frac{\partial}{\partial x_i}(\rho\varepsilon U_i) = \frac{\partial}{\partial x_j}\left[\left(\mu + \frac{\mu_t}{\sigma_\varepsilon}\right)\frac{\partial \varepsilon}{\partial x_j}\right] + \rho C_1 S\varepsilon - \rho C_2 \frac{\varepsilon^2}{k + \sqrt{\nu\varepsilon}} + C_{1\varepsilon}\frac{\varepsilon}{k}C_{3\varepsilon} \tag{13}$$

where G_k represents the the generation term, terms as C_1 are constants, σ_k and σ_ε represent the Prandtl number for both k and ε.

2.2. Domain and mesh

Carraretto et al. (2020) in their experimental setup employed a 24-meter long pipeline, a domain that would be excessively demanding for a detailed numerical simulation. Therefore, in this study only a portion of the pipe used in experiments is simulated to reduce the computational cost. For the purpose of sensitivity analyses, a 2-meter pipe and a 3-meter one were considered. Given the inner diameter of 60 mm, the domain is long enough to ensure complete flow development since the length is greater than 10 diameters. A fine, structured mesh with hexahedral cells is used for the computations. Additional refinement near the wall was used to correctly resolve the boundary layer. Also, dynamic grid refinement at the gas-liquid interface was performed every 20 timesteps to increase the level of accuracy. The refinement criterion is based on "field variable registers" that allows marking the cells based on the value of a field variable. In this work, the gradient-based approach to mark the cells was adopted. According to ANSYS (2019), Ansys Fluent multiplies the Euclidean norm of the gradient of the selected solution variable by a characteristic length scale to define the adaption function. For example, the gradient function in three dimensions has the following form:

$$|e_i| = (V_{cell})^{1/3}|\nabla f| \tag{14}$$

where e_i is the error indicator, V_{cell} is the cell volume and $|\nabla f|$ is the Euclidean norm of the gradient of the desired field variable. The value of e_i is then scaled by its global maximum in the domain such that $0 < e_i < 1$. If $e_i < 5 \cdot 10^{-5}$ or $e_i > 2.5 \cdot 10^{-2}$ cells are coarsened or refined respectively. This condition ensures an optimal mesh refinement around the interface as showed in Fig. 2. For more information regarding cell splitting algorithms please refer to ANSYS (2019).

The influence of mesh density on the accuracy of the results was also object of the study. Four meshes with increasing refinement were generated to assess this effect. The details of all the grids are given in Table 1 while an image of the mesh adopted during computations is showed in Fig. 2.

2.3. Solver setup

The software Ansys Fluent 2019 R3 was used for the simulations. As already mentioned, the multiphase model adopted was the Volume of Fluid because of its ability to

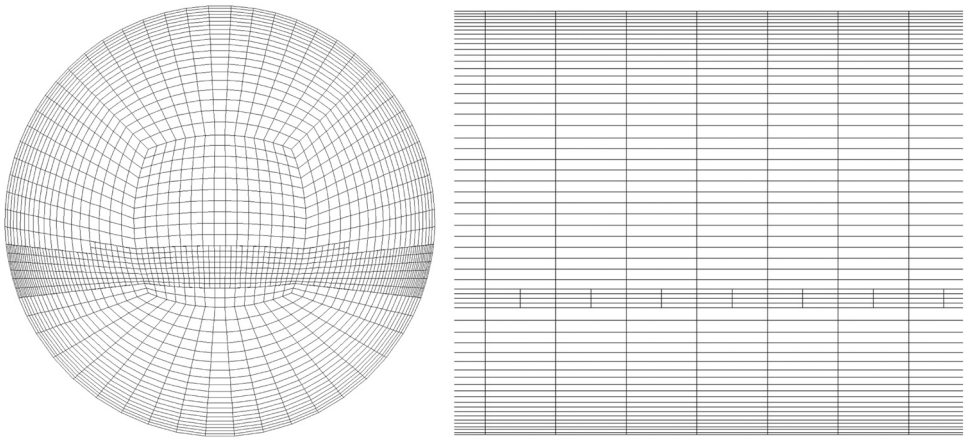

Fig. 2 – Discretization grid with dynamic mesh adaption at the interface: Cross-section (*a*) and section along the axis (*b*).

Table 1 – Details of mesh metrics.

Mesh density level	1	2	3	4
Cells on cross section [elements]	446	698	1105	1480
Axial spacing [mm]	5	4	3	2
Total number of cells [10^3 elements]	178	349	737	1480

capture the interface between two immiscible fluids. Liquid water and air are set as primary and secondary phases, respectively. Turbulence models were implemented with a y^+-insensitive near-wall modeling approach. This method combines a two-layer model with so-called enhanced wall functions. If the near-wall mesh is fine enough to be able to resolve the viscous sublayer, then the enhanced wall treatment will be identical to the traditional two-layer zonal model. However, the restriction that the near-wall mesh must be sufficiently fine everywhere might impose too large a computational requirement. ANSYS Fluent can combine the two-layer model with enhanced wall functions that provide a smooth transition from viscous sublayer to log-law region. ANSYS (2019). Phases thermo-physical properties were considered constant and are reported in Table 2. Surface tension is modeled with a "Continuum Surface Force" (CSF) approach as described in Brackbill et al. (1992). The inlet section was divided in two surfaces in order to provide boundary conditions for both fluids: air and water enter the pipe from upper and lower part of the inlet cross section, respectively. This division was done taking into account the average interface height from experiments. Outlet boundary condition was set as "outflow", a particular condition that can be used to model flow exits where velocity and pressure are not known prior to solving the problem (ANSYS, 2019). The authors benchmarked also the "pressure outlet" boundary condition, but it resulted in a non-physical pressure field since it applies a constant pressure profile on the outlet surface without considering the change due to the different hydrostatic head among the two phases.

Regarding discretization schemes, the Second Order Upwind method is chosen for spatial discretization of momentum, turbulence and transition quantities (k, ε, ω, γ and $Re_{\theta t}$) because of higher accuracy compared with first order schemes. Pressure was discretized with PRESTO! algorithm

Table 2 – Summary of the simulation settings in ANSYS Fluent.

Solver	Pressure-based Type - Absolute Velocity Formulation Transient time scheme
Multiphase Model	Volume Of Fluid (VOF) with Explicit formulation - Implicit Body Force Sharp Interface Modeling - Interfacial Anti-Diffusion
Phase-Interaction	Surface Tension Force Modelling (CSF) Constant Surface Tension Coefficient = 0.073 N/m
Viscous Model	Transition SST / Realizable k-ε / SST k-ω Default model constants, y^+-insensitive wall treatment
Boundary Conditions	Inlet: actual phase velocity $(J/\epsilon)_{exp}$ for gas and liquid imposed with a constant profile Inlet Turbulence: 5 % turbulence intensity and hydraulic diameter Outlet: Outflow Wall: Stationary - No Slip Condition
Operating Conditions	Atmospheric Pressure Gravity = – 9.81m/s^2 in Y Direction, Operating density = 1.2 kg/m^3
Material Properties	ρ_{gas} = 1.2kg/m^3, μ_{gas} = 1.7894e – 05$kg/(m \cdot s)$ ρ_{liquid} = 998.2kg/m^3, μ_{liquid} = 0.001$kg/(m \cdot s)$
Solution Methods	Pressure-Velocity Coupling: PISO Spatial Discretization of Pressure: PRESTO! Spatial Discretization of Volume Fraction: Geo-reconstruct Gradients: Least-squares cell based Other Variables: Second order upwind

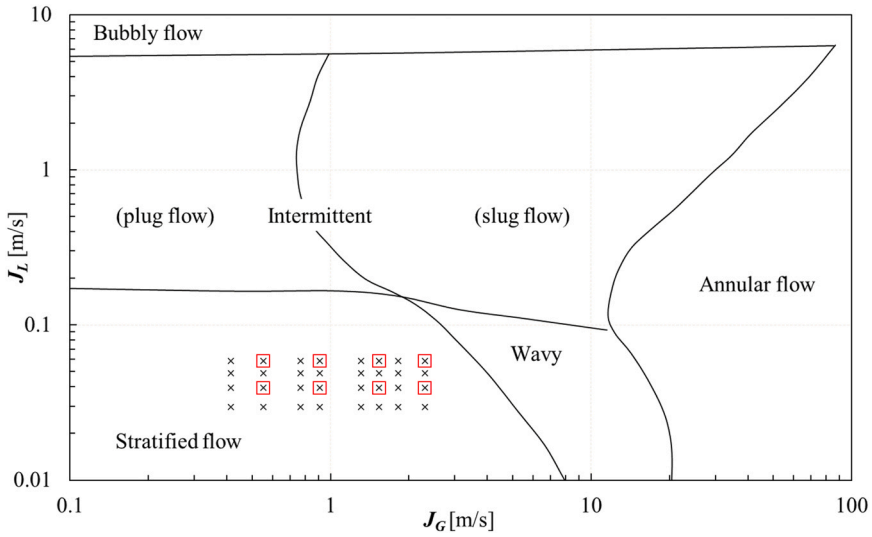

Fig. 3 – Mandhane map for horizontal pipes. Experimental data by Carraretto et al. (2020) indicated with crosses. Simulated experimental points are highlighted with a red square.

and gradients with the least-squares cell based methodology. PISO scheme was used for the pressure-velocity coupling operation.

All the simulations were initialize with Fluent's "Hybrid Initialization" then the liquid phase volume fraction was patched to the domain to position the interface at the defined height according to the inlet section. A constant velocity field was applied to liquid and gas velocity. All the cases have then been run for 35 s of flow-time to guarantee a more than one turnover time (i.e. the time it take to propagate an information from inlet to outlet section) for the liquid phase which the slowest one. Such flow-time has been chosen by monitoring the pressure gradient throughout the simulation and waiting for its stabilization. The transient timestep is variable and it is adapted during the simulation to maintain the VOF Courant number below 0.5. The choice of a transient solver is a consequence of both using the explicit formulation of VOF model and using the most accurate scheme for interface tracking: the Geometrical Reconstruction, Youngs (1982). Simulation residuals were monitored in order to asses convergence of each timestep. A summary of all the simulation settings is given in Table 2.

2.4. *Validation procedure*

To validate the numerical results, a total of eight experimental points by Carraretto et al. (2020) were considered as benchmark. Fig. 3 show the flow regime map where the experimental point are highlighted. Table 3 summarizes instead the details of the investigated cases. This table reports the values of gas and liquid superficial velocity (J_g and J_L [m/s]), the void fraction (ϵ [–]), the experimental value of pressure gradient ($(-dp/dx)_{exp}$ [Pa/m]), the hydraulic diameter for gas phase ($D_{h,g}$ [m]) and a Reynolds number defined as $Re_g = \frac{\rho V_g D_{h,g}}{\mu}$[–] where the actual gas velocity is given by $U_g = J_g/\epsilon$ [m/s]. This dimensionless number can be used as an approximate indicator of the level of turbulence in gas phase. According to the values reported in Table 3, it can be said that cases 1 and 5 are in transition regime from laminar to turbulent, cases 3, 4, 7 and 8 are in the fully turbulent regime while cases 2 and 6 rely in what can be called "mildly turbulent" zone right after transition. This subdivision will be important for the turbulence model selection as it will be shown in the next section. Since the accurate investigation of the pressure drop in the pipe is the main purpose of this work, the pressure was monitored in 21 points in the domain distanced 250 mm one another along the X coordinate (pipe axis direction). Their position on Y axis is similar to the one of the pressure probes used in the experiments. They were placed at the center of the pipe (Z = 0) and distanced 5 mm form top surface. Pressure data were time-averaged for the last 5 s of each simulation and the pressure gradient was calculated by linear interpolation of these data along pipe axis. In order to eliminate the effect of boundary conditions, the first and the last 250 mm of the domain length were excluded from the regression procedure. The values obtained in

Table 3 – Summary of validation targets.

Case	J_g [m/s]	J_L [m/s]	ε_{exp} [–]	$(-dp/dx)_{exp}$ [Pa/m]	$D_{h,g}$ [m]	Re_g [–]
1	0.551	0.040	0.705	0.486	0.047	2417
2	1.308	0.040	0.743	1.958	0.048	5650
3	1.538	0.040	0.753	2.650	0.049	6618
4	2.306	0.040	0.772	5.010	0.050	9851
5	0.551	0.060	0.623	0.670	0.043	2471
6	1.308	0.060	0.698	2.631	0.046	5694
7	1.538	0.060	0.708	3.418	0.047	6677
8	2.306	0.060	0.728	6.105	0.048	9923

Table 4 – Summary of mesh density analysis.

Mesh density level	$(-dp/dx)_{num}$ [Pa/m]	$(-dp/dx)_{exp}$ [Pa/m]	Percentage error [%]
1	0.3981	0.486	– 18.08 %
2	0.4031	0.486	– 17.06 %
3	0.4289	0.486	– 11.74 %
4	0.4588	0.486	– 5.60 %

this way for the different simulations, were then compared to experimental data. The percentage error used to describe the accuracy of the prediction was defined as:

$$e\% = \frac{(-dp/dx)_{num} - (-dp/dx)_{exp}}{(-dp/dx)_{exp}} \cdot 100 \quad (15)$$

3. Sensitivity analyses and validation

3.1. *Effect of grid refinement and turbulence models*

Sensitivity analyses on grid refinement and turbulence model are necessary to completely define the simulation methodology. As already mentioned in Section 2.2, four meshes with an increasing level of refinement were created. In order to evaluate their influence on the results, case 1 was simulated on a 2-meter long domain with Transition SST turbulence model on all four grids. The resulting pressure gradient was evaluated and compared to experimental values. Table 4 summarizes the outcome of this analysis. Results show that mesh density plays an important role in the accuracy of the prediction. Accordingly, mesh density level 4 (ref. Table 1) was chosen for all the further simulations. It is worth noting that all the turbulence model tested were implemented with a y^+ insensitive wall treatment. Nevertheless, the employed meshes ensure a y^+ lower than 5 for all the test cases. Moreover, the influence of axial spacing was also tested. Starting from mesh density level 4 (ref. Table 1, the axial spacing was relaxed from 2 mm to 10 mm in 5 steps and a 1.15 % difference in accuracy was observed going from the finest to the coarsest spacing. Therefore, the authors concluded that the axial grid spacing could be relaxed to some extent without a significant loss in accuracy but with a great saving in computational time. Hence, the larger axial spacing of 10 mm was taken as reference for all the further simulations. Lastly, domain extent was examined. The mesh just described was employed to discretize a 2-meter long domain and a 3-meter long one. The absolute value of the error was asymptotic, but to be on the safe side a 3-meter long domain was preferred in order to evaluate the pressure gradient on a total length that was about 10 % of the pipe used in the experiments.

Defined the domain and mesh to be used, the influence of turbulence models needs to be assessed. As reported in Section 3, different turbulent regimes are present in the experiments. As a results, transition, fully turbulent or both models could be used to simulate the experimental points. In particular, three aspects must be investigated: the accuracy of transition SST model in the fully turbulent regime, the accuracy of a fully turbulent model in the transition regime and which model is more accurate between Realizable k-ε SST k-ω and Transition SST for the highest gas velocities. To this aim, at first the three models were compared on case 4 (fully turbulent regime), then the transition SST was compared against the most accurate between the previous ones on case 2 to assess the performance of the models right after transition to turbulent flow and at last, the chosen fully turbulent model was employed to simulate the transition regime. Table 5 summarizes the outcome of these analyses.

Data show that Realizable k-ε is significantly more accurate than SST k-ω in the fully turbulent regime, with a percentage error on pressure gradient of –19.81 % against –50.61 % respectively. Comparing instead the Transition SST model to Realizable k-ε, it can be noted that both reach the same level of accuracy in the fully turbulent regime while k-ε exhibits a lower percentage error in what the author called "mildly turbulent" region. At constant liquid superficial velocity, the Transition SST model would be able to cover the entire range of increasing gas superficial velocity but, for a higher accuracy, it is preferable to use a fully turbulent model right after the transition to turbulent regime. Finally, the comparison between Transition SST and Realizable k-ε showed that the first must be preferred for the transition zone since the second is very inaccurate with an error of +71.43 %. The authors have therefore decided to use the Transition SST model just for cases 1 and 5 and Realizable k-ε for all the others.

3.2. *Validation*

The experimentally obtained data on pressure gradient and void fraction were used as metrics to assess the accuracy of the simulations. Focusing on the pressure gradients, as reported in Table 6, numerical simulations tend to underestimate the experimental values (MRD = – 11.32 % and MARD = 12.39 %). Referring to Fig. 4 two different representations of the CFD simulation accuracy are provided: in the first one (Fig. 4a) the predicted pressure gradient is reported against the experimental data in a parity plot, while in the second one (Fig. 4b) the percentage error is displayed

Table 5 – Results of turbulence model sensitivity analysis.

Case	Turbulence model	$(-dp/dx)_{num}$ [Pa/m]	$(-dp/dx)_{exp}$ [Pa/m]	Percentage error [%]
4	Transition SST	4.0498	5.010	– 19.17 %
4	Realizable k-ε	4.0174	5.010	– 19.81 %
4	SST k-ω	2.4746	5.010	– 50.61 %
2	Transition SST	1.7617	1.958	– 10.02 %
2	Realizable k-ε	1.9132	1.958	– 2.29 %
1	Realizable k-ε	0.8332	0.4860	71.43 %
1	Transition SST	0.5069	0.4860	4.29 %

Table 6 – Results of CFD simulations.

Case	$(-dp/dx)_{num}$ [Pa/m]	$(-dp/dx)_{exp}$ [Pa/m]	Error [%]	ε_{num} [–]	ε_{exp} [–]	Error [%]
1	0.5069	0.486	4.29 %	0.715	0.705	+1.41 %
2	1.9132	1.958	– 2.29 %	0.717	0.743	– 3.54 %
3	2.4401	2.650	– 7.92 %	0.714	0.753	– 5.18 %
4	4.0174	5.010	– 19.81 %	0.713	0.772	– 7.68 %
5	0.6078	0.670	– 9.28 %	0.685	0.623	+9.97 %
6	2.2330	2.631	– 15.13 %	0.667	0.698	– 4.43 %
7	2.7934	3.418	– 18.27 %	0.670	0.708	– 5.30 %
8	4.2176	6.105	– 22.15 %	0.664	0.728	– 8.76 %

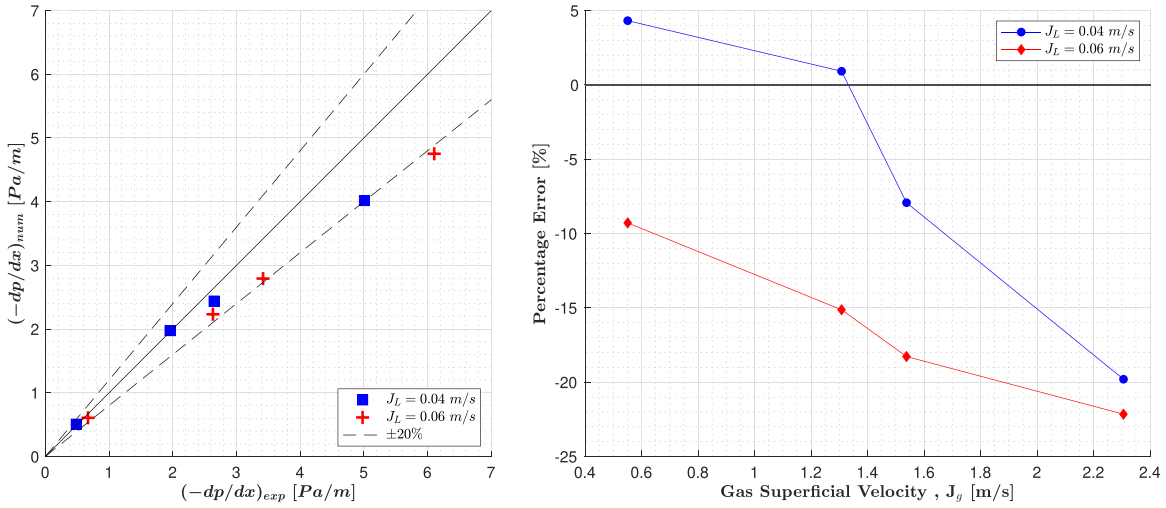

(a) Parity plot, ±20% error band

(b) Trend of percentage error

Fig. 4 – Representation of numerical simulation accuracy.

as function of the superficial gas velocity. The percentage error trend is analogous for the two conditions considered and always included in the ± 20 % error region. In particular, the prediction worsen as the gas superficial velocity increases. The same behavior can be observed for void fraction.

Fig. 5 displays the air volume fraction contour in four different cases: lowest and highest Reynolds numbers for the two different liquid superficial velocities analyzed. It is evident that no ripples on the interface are present thus resulting in a stratified flow regime.

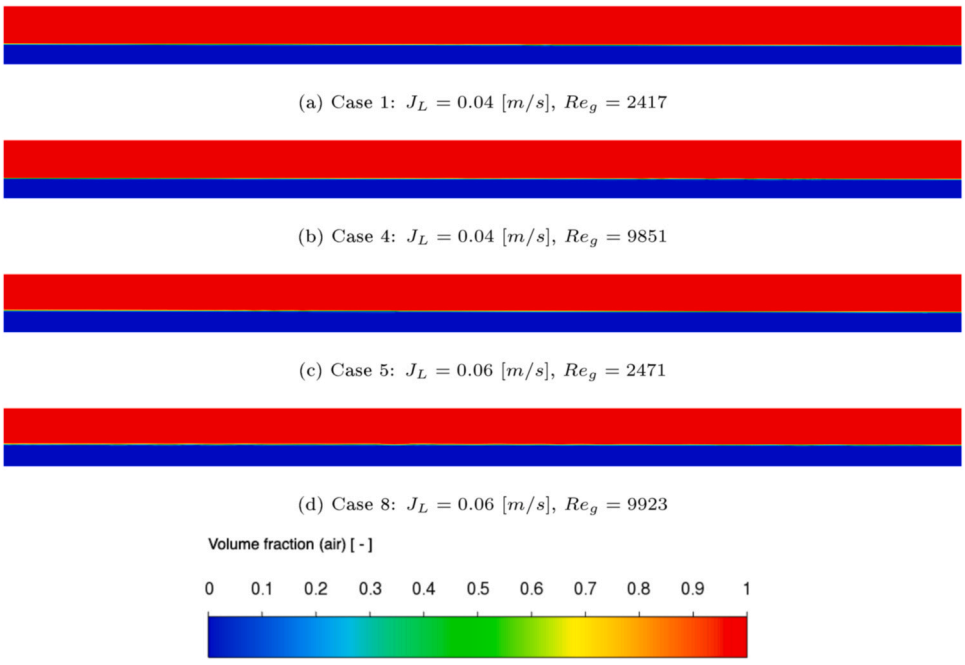

(a) Case 1: $J_L = 0.04\ [m/s]$, $Re_g = 2417$

(b) Case 4: $J_L = 0.04\ [m/s]$, $Re_g = 9851$

(c) Case 5: $J_L = 0.06\ [m/s]$, $Re_g = 2471$

(d) Case 8: $J_L = 0.06\ [m/s]$, $Re_g = 9923$

Fig. 5 – Air void fraction contour in a central section of the pipe, $x \in [1,2]$ m.

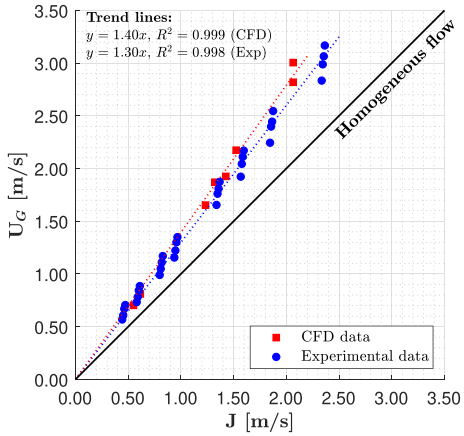

(a) Effective gas velocity average mixture superficial velocity

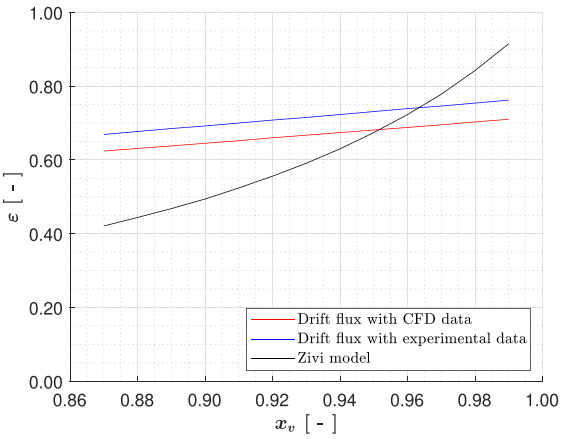

(b) Void fraction comparison for J_L=0.06 m/s

Fig. 6 – Void fraction analysis. Experimental data from Carraretto et al. (2020).

4. Results and discussion

Hence, the obtained results were first elaborated according to Zuber and Findlay (1965) drift flux, which is well-known in the open literature to be both a practical and accurate model for two-phase flow analysis. Then the data were compared to the ones obtained fitting the experimental values with the same model. The reader might refer to Carraretto et al. (2020) for a detailed analysis about the drift flux derivation.

In Fig. 6a, the effective gas velocity ($U_G = J_G/\varepsilon$ [m/s]) is plotted against the mixture velocity $J = J_L + J_G$ [m/s]. For the CFD simulation, the void fraction ε [–] was computed as the averaged ratio of gas and liquid areas in different cross-section along the pipe axis. The two datasets are linearly correlated. The slope of these lines is the "distribution parameter (C_0)", that accounts for non-uniform distribution of the two phases. The two models agree with respect to each other having a Mean Absolute Relative Deviation (MARD) of 6.30 %. In both cases the drift velocity is zero, as expected for horizontal flows (Crowe, 2005). On the other hand, the two distribution parameters are slightly different, i.e., 1.30 and 1.40 for experimental data and CFD simulations, respectively. However, the major deviation is found at the highest mixture velocities, where also the pressure gradient is significantly underpredicted by the best CFD model.

Accordingly, CFD underestimates void fraction by about 14 %, but is able to reproduce the same trend against volume quality as the experimental data, shown in Fig. 6b, where the predicted void fraction is plotted against volumetric quality. The plot also reports for the sake of comparison the prediction by the Zivi (1964) correlation, which Márquez-Torres et al. (2020) report as the best predictor for stratified flows with liquid viscosity equal or lower than 1 *cP*. However, it should be kept in mind that such a model has not been derived specifically for stratified flows and is implicitly based on the assumption of constant slip ratio (equal to about 9 in the present conditions). It is then not surprising that there is no agreement with either experimental data or CFD simulations in spite of the acceptable statistical performance of the Zivi (1964) correlation over the broad range of data examined by Márquez-Torres et al. (2020).

As reported in section 3, simulations tend to underestimate the pressure gradient. Such a behaviour is opposite to the one shown by the 1D models reviewed from the open literature (Cohen and Hanratty, 1968; Agrawal et al., 1973; Taitel and Dukler, 1976; Cheremisinoff and Davis, 1979; Kowalski, 1987; Crowley et al., 1992; Ullmann and Brauner, 2006). Their performance is compared in Fig. 7 where it is evident that they strongly overestimate the pressure gradient in the lower range of the gas superficial velocity. The agreement significantly improves as J_g increases. In

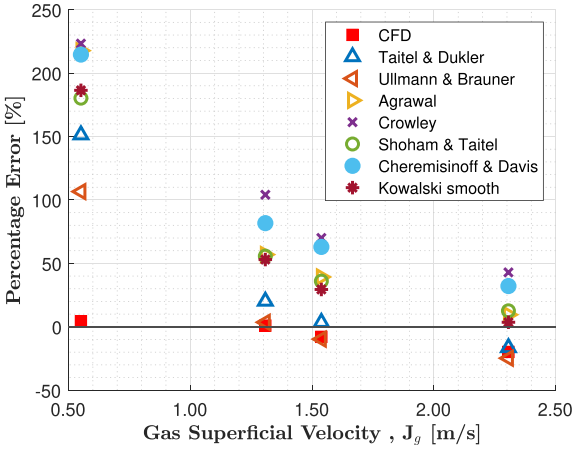

(a) Liquid superficial velocity = 0.04 m /s

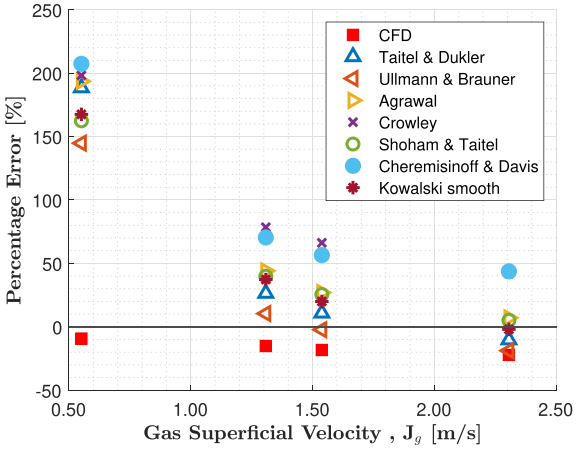

(b) Liquid superficial velocity = 0.06 m /s

Fig. 7 – Percentage error of numerical results and 1D pressure gradient predictions with respect to experimental values.

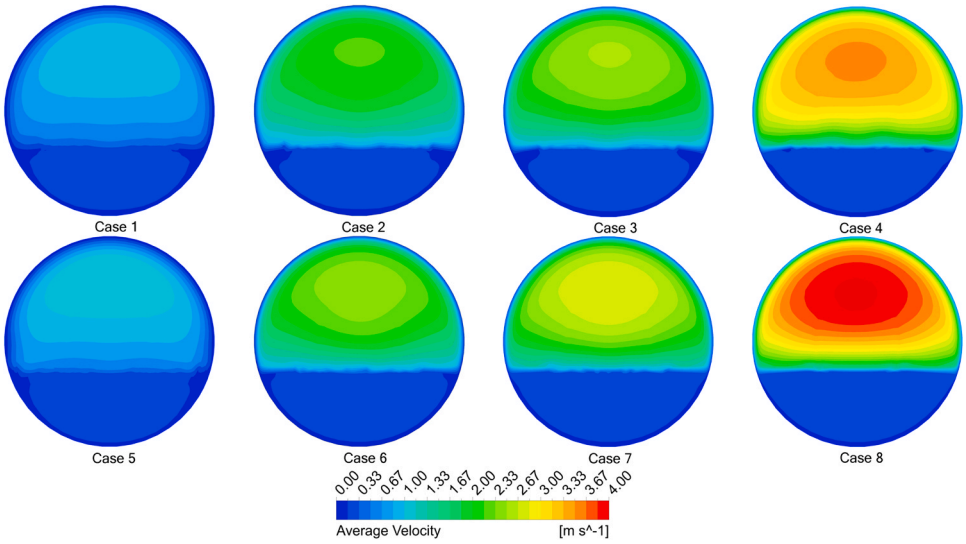

Fig. 8 – Cross-sectional velocity contour for the different cases.

particular, the Ullmann and Brauner (2006) model gives a prediction comparable with the CFD simulations at the lowest liquid superficial velocity and shows an even superior performance at the highest liquid superficial velocity for $J_g > 1.3$ *m/s*. The classic Taitel and Dukler (1976) model shows a quite similar behaviour, being the base for the Ullmann and Brauner (2006) model, and results the second best predictor.

Hence, from both void fraction and pressure gradient analysis, it appears that the CFD simulations can overcome the 1D models limitations, reducing the discrepancies with the experimental results and can help revealing 1D models bottlenecks. Specifically, the prediction error might be linked to oversimplifying assumptions in the formulation of both the wall and the interfacial shear stress. Actually, the former is evaluated for each phase from the gas and liquid friction factors correlations established for single-phase flow in circular pipes: generalization is simply obtained by adopting the hydraulic diameter in the assumption that the interface is seen as a wall on the gas side. However, the velocity profiles are quite different from the ones relative to the single-phase flow. Fig. 8 shows the velocity contours on the cross-section, exhibiting a symmetry about the vertical midplane rather than a radial symmetry as in the single-phase flow.

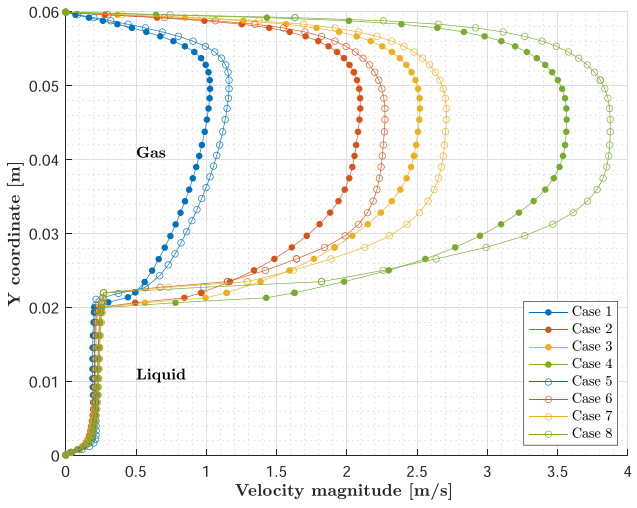

Fig. 9 – Velocity profiles along pipe axis at its center for the different cases.

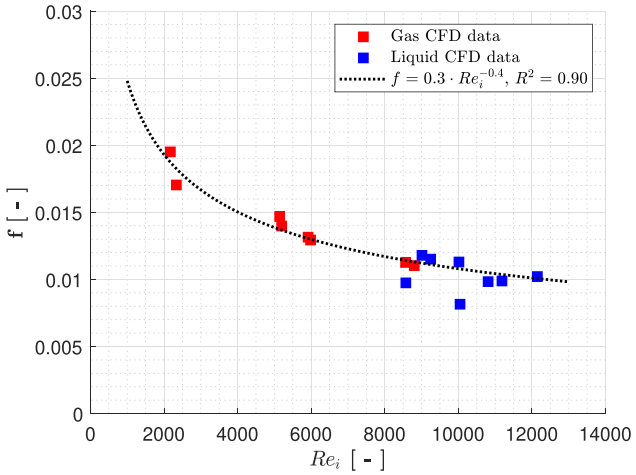

Fig. 10 – Friction factor versus phase Reynolds number: i stands for either gas (red markers) or liquid (blue markers).

Instead, Fig. 9 provides the velocity profiles at the vertical midplane, where both the phases reach the maximum local velocity: it is observed that the assumption that the interface is seen as a wall by the gas holds with a larger margin as the gas velocity increases; actually, the gas velocity profile is more and more symmetric about the horizontal plane as the velocity increases. On the other hand, the shape of the liquid velocity profile is not significantly affected by the gas velocity apart from the slight variation in the interface position due to the change in the void fraction. In any case, a distortion of the velocity profile in both phases is expected compared to the single-phase ones, which causes the wall shear stress to be unevenly distributed along the circumference. Accordingly, the average wall shear stress - usually expressed in dimensionless form by the friction factor - is far from being represented in terms of the typical Blasius-type relationships adopted for single phase flows.

This is clearly seen in Fig. 10 where the Fanning friction factor computed from the average wall shear stress and the average phase velocity obtained from simulations is reported against the phase Reynolds number for both the gas and the liquid: the computed values are fairly well represented by the power law typical of Blasius-type models, but with

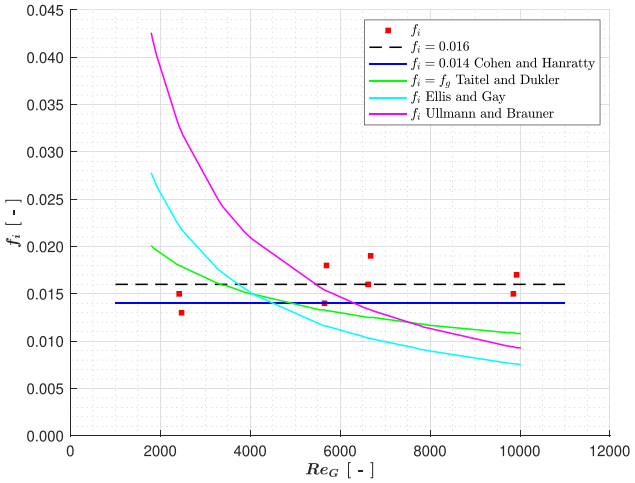

Fig. 11 – Interfacial friction factor vs. Reynolds number.

significantly higher coefficient and exponent. Hence, the actual friction factor is from about 50–80 % higher than in the case of single-phase flow.

Eventually, replacing the actual friction factor in the 1D two-fluid model with the measured pressure gradients (Eqs. (2) and (3)), the average interfacial shear stress is easily derived, thus the corresponding interfacial friction factor is evaluated as:

$$f_i = \frac{2\tau_i}{\rho_g (U_g - U_L)^2} \tag{16}$$

where τ_i is the interfacial shear stress obtained from simulations. The obtained interfacial friction factor values are plotted as a function of the gas Reynolds number in Fig. 11. The computed values appear independent of the Reynolds number with an average of 0.016. This result is very similar to the findings of Cohen and Hanratty (1968) who measured the interfacial shear stress in fully developed stratified flows in a flat channel, obtaining for the interfacial friction factor a constant value of about 0.014 in a broad range of operating conditions (the reader is warned that in the cited work the Darcy friction factor is used instead of the Fanning one: the reported value is consistent with the adoption of the latter in this paper). The Figure also shows the comparison with the interfacial friction factors according to Taitel and Dukler (1976), Ellis and Gay (1959) and Ullmann and Brauner (2006) adopted in the two-fluid models reviewed in Section 1: though on the average the values are in agreement, the interfacial friction factor is significantly overestimated for $Re_G < 4000$ and underestimated for $Re_G > 6000$.

5. Conclusions

This work was aimed at defining a numerical methodology for a better prediction of both the pressure gradient and void fraction provided of two-phase stratified flow in horizontal pipes. Sensitivity analyses on mesh refinement, domain size and turbulence model were conducted to understand their influence on the results. The outcome of the simulations was then compared against experimental data from Carraretto et al. (2020) for validation purposes. The problem was modeled by unsteady, multiphase CFD simulation. The Volume Of Fluid method was used to track the interface between the two phases. The sensitivity analyses showed that mesh refinement has a significant impact on the accuracy of the simulation. A fine mesh is needed especially on the cross-section while the axial spacing can be coarsened to reduce the computational cost without losing accuracy. Even though Transition SST was able to guarantee a great accuracy for all the increasing gas superficial velocities, Realizable k-ε was employed after laminar to turbulent transition to achieve a greater overall accuracy of the predictions. Results showed a general underestimation of the pressure gradient with an average error of – 6.43 % and – 16.21 % for liquid superficial velocities of 0.04 m/s and 0.06 m/s, respectively. Concerning the void fraction, a good agreement between experimental results and CFD simulations was found. In both cases a drift flux model was implemented and a MARD of 6.30 % was computed. The results were also compared with prediction from 1D two-fluid models showing that CFD has a superior performance especially at low gas superficial velocities. Two major causes of disagreement were found in the basic assumptions of the 1D two-fluid models: first, the adoption of single-phase Blasius-type correlations for the phase friction factors, which leads to a wrong estimation of the wall shear stress; second, the use of empirical correlations for the interfacial friction factor, which are still lacking in terms of both validation and generalization. As a further development, the simulated operating conditions could be expanded by further increasing the gas velocity and moving from stratified to wavy regime.

Declaration of Competing Interest

The authors declare that they have no known competing financial interests or personal relationships that could have appeared to influence the work reported in this paper.

Acknowledgements

The authors want to acknowledge the CFDhub of Politecnico di Milano (https://www.cfdhub.polimi.it) for providing the computational resources needed for the completion of this work.

References

Agrawal, S.S., Gregory, G.A., Govier, G.W., 1973. An analysis of horizontal stratified two phase flow in pipes. Can. J. Chem. Eng. 51, 280–286.

ANSYS, 2019.Ansys fluent theory guide release 2019 R3.ANSYS Inc.

Arabi, A., Azzi, A., Kadi, R., Al-Sarkhi, A., Hewakandamby, B., 2021. Empirical modelization of intermittent gas/liquid flow hydrodynamic parameters: The importance of distinguishing between plug and slug flows. SPE Prod. Oper. 36, 703–720.

Banerjee, R., Isaac, K.M., 2003.Evaluation of Turbulence Closure Schemes for Stratified Two Phase Flow, pp.689–705.

Brackbill, J.U., Kothe, D.B., Zemach, C., 1992. A continuum method for modeling surface tension. J. Comput. Phys. 100, 335–354.

Brauner, M.M., 1991. Analysis of stratified/nonstratified transitional boundaries in horizontal gas-liquid flows. Chem. Eng. Sci. 46, 1849–1859.

Brennen, C.E., 2005. Fundamentals of Multiphase Flow. Cambridge University Press.

Carraretto, I.M., Colombo, L.P.M., Fasani, D., Guilizzoni, M., Lucchini, A., 2020. Pressure drop and void fraction in horizontal air-water stratified flows with smooth interface at atmospheric pressure. Fluids 5.

Cheremisinoff, N.P., Davis, E.J., 1979. Stratified turbulent-turbulent gas-liquid flow. AIChE J. 25, 48–56.

Chinello, G., Ayati, A.A., McGlinchey, D., Ooms, G., Henkes, R., 2018. Comparison of computational fluid dynamics simulations and experiments for stratified air-water flows in pipes. J. Fluids Eng. 141.
Cohen, L.S., Hanratty, T.J., 1968. Effect of waves at a gas—liquid interface on a turbulent air flow. J. Fluid Mech. 31, 467–479.
Crowe, C.T., 2005. Multiphase Flow Handbook. CRC Press.
Crowley, C., Wallis, G., Barry, J., 1992. Validation of a one-dimensional wave model for the stratified-to-slug flow regime transition, with consequences for wave growth and slug frequency. Int. J. Multiph. Flow. 18, 249–271.
Dabirian, R., Mansouri, A., Mohan, R., Shoham, O., Kouba, G., 2015.CFD Simulation of Turbulent Flow Structure in Stratified Gas/Liquid Flow and Validation with Experimental Data.
Ellis, S., Gay, B., 1959. The parallel flow of two fluid streams: interfacial shear and fluid-fluid interaction. Trans. Instn. Chem. Engrs 37, 206–213.
Govier, G.W., Aziz, K., 1972. The Flow of Complex Mixtures In Pipes. Van Nostrand Reinhold New York.
Govier, G.W., Aziz, K., Schowalter, W.R., 1973. The flow of complex mixtures in pipes. J. Appl. Mech. 40 404-404.
Kowalski, J.E., 1987. Wall and interfacial shear stress in stratified flow in a horizontal pipe. AIChE J. 33, 274–281.
Lockhart, R.W., 1949. Proposed correlation of data for isothermal two-phase, two-component flow in pipes. Chem. Eng. Prog. 45, 39–48.
Mandhane, J., Gregory, G., Aziz, K., 1974. A flow pattern map for gas—liquid flow in horizontal pipes. Int. J. Multiph. Flow. 1, 537–553.
Márquez-Torres, L., Ochoa-Pineda, J., Pico, P., Valdés, J.P., Becerra, D., Pinilla, A., Pereyra, E., Ratkovich, N., 2020. Comparison of 63 different void fraction correlations for different flow patterns, pipe inclinations, and liquid viscosities. SN Appl. Sci. 2, 1695.
Menter, F.R., 1994. Two-equation eddy-viscosity turbulence models for engineering applications. AIAA J. 32, 1598–1605.
Miya, M., Woodmansee, D.E., Hanratty, T.J., 1971. A model for roll waves in gas-liquid flow. Chem. Eng. Sci. 26, 1915–1931.
Mokhatab, S., Poe, W.A., 2012. Handbook of Natural Gas Transmission and Processing. Gulf professional publishing.
Russell, T., Etchells, A., Jensen, R., Arruda, P., 1974. Pressure drop and holdup in stratified gas-liquid flow. AIChE J. 20, 664–669.
de Sampaio, P.A., Faccini, J.L., Su, J., 2008. Modelling of stratified gas–liquid two-phase flow in horizontal circular pipes. Int. J. Heat. Mass Transf. 51, 2752–2761.
Shih, T.H., Liou, W.W., Shabbir, A., Yang, Z., Zhu, J., 1995. A new k-ϵ eddy viscosity model for high reynolds number turbulent flows. Comput. Fluids 24, 227–238.
Taitel, Y., Dukler, A.E., 1976. A model for predicting flow regime transitions in horizontal and near horizontal gas-liquid flow. AIChE J. 22, 47–55.
Tzotzi, C., Bontozoglou, V., Andritsos, N., Vlachogiannis, M., 2011. Effect of fluid properties on flow patterns in two-phase gas-liquid flow in horizontal and downward pipes. Ind. Eng. Chem. Res. 50, 645–655.
Ullmann, A., Brauner, N., 2006. Closure relations for two-fluid models for two-phase stratified smooth and stratified wavy flows. Int. J. Multiph. Flow. 32, 82–105.
Ullmann, A., Goldstein, A., Zamir, M., Brauner, N., 2004. Closure relations for the shear stresses in two-fluid models for laminar stratified flow. Int. J. Multiph. Flow. 30, 877–900.
Youngs, D.L., 1982. Time-dependent multi-material flow with large fluid distortion. Numer. Methods Fluid Dyn.
Zivi, S.M., 1964. Estimation of steady-state steam void-fraction by means of the principle of minimum entropy production. J. Heat. Transf. 86, 247–251.
Zuber, N., Findlay, J.A., 1965. Average volumetric concentration in two-phase flow systems. J. Heat. Transf. 87, 453–468.